

A mathematical model of intervillous blood flow in the human placentone

Igor L. Chernyavsky^a, Oliver E. Jensen^a, Lopa Leach^b

^a*Centre for Mathematical Medicine and Biology, School of Mathematical Sciences, University of Nottingham, University Park, Nottingham NG7 2RD, UK*

^b*Centre for Integrated Systems Biology and Medicine, School of Biomedical Sciences, University of Nottingham, Queen's Medical Centre, Nottingham NG7 2UH, UK*

Abstract

We present a mathematical model for maternal blood flow in a placental circulatory unit (a placentone), describing flow of maternal blood via Darcy's law and steady advective transport of a dissolved nutrient. The method of images and computational integration along streamlines are employed to find flow and solute concentration distributions, which are illustrated for a range of governing system parameters. The model shows how the calibre of the basal vessels can be a dominant determinant of the maternal blood flow rate through the placentone, given a driving pressure difference between the spiral arteries and decidual veins. The model supports the hypothesis that basal veins are located on the periphery of the placentone in order to optimise delivery of nutrients and suggests the existence of an optimal volume fraction of villous tissue.

Key words: placentone, intervillous blood flow, method of images, solute transport, optimal uptake

1. Introduction

Our modern understanding of blood flow in the primate and human placenta is based on the pioneering studies by Freese, Ramsey, Reynolds, Wilkin and Wigglesworth [1–5]. Using a combination of radioangiography and casting techniques they visualised the flow patterns of maternal blood and the morphological relationship between the uteroplacental vasculature and fetal chorionic villi. Here, we will use mathematical modelling to characterise some of the primary physiological features of maternal placental blood flow.

The functional circulatory unit of the human placenta, a “placentone,” is defined as a single fetal villous tree and its corresponding decidual vessels. Maternal blood, ejected from a spiral artery, passes between the branches of the villous tree before leaving the

placentone through decidual veins. Although strict anatomic borders cannot always be found between these functional units [6], this arrangement is most clear in the peripheral lobes of the mature human placenta [7]. The distinguishing features of the placentone are a central cavity of the fetal villous tree with less differentiated villi, a dense lateral portion, the functional decidual arterial opening into the central cavity, and basal venous openings near the periphery [6, 8] (Fig. 1).

The problem of obtaining a quantitative statistical description of the distribution of decidual vasculature over the basal plate is still open (see [7] for a review), although the number of functional openings of spiral arteries is thought to be comparable with the number of fetal villous trees in the mature placenta [9]. There are three main hypotheses for the distribution of venous openings: random; concentrated near placental margins; and concentrated in the periphery of placentones and near the placental septa [9]. The last hypothesis is the closest to current views [7] and it is analysed in the present work by means of a mathematical model.

Mathematical models can assist in investigating the impact of basal vasculature distribution on intervillous blood flow and solute uptake, since the placental structure of each species will have evolved to optimise its functions against certain constraints [10]. Theoretical studies of the placental circulation and metabolic exchange were started more than 40 years ago by Faber, Kirschbaum, Longo, Moll and co-workers [11–14]. Nevertheless, we still do not have complete understanding of many phenomena related to intrauterine fetal growth restriction and macrosomia, and it is also unclear how these pathologies are connected to placental structure, haemodynamics and regulatory activity.

The first compartmental models focused on oxygen and carbon dioxide exchange between the maternal and fetal circulatory systems, ignoring spatial flow patterns of maternal blood, where Fick’s law was used to approximate diffusive mass transfer across the placental barrier [11, 12, 15, 16]. Later approaches, such as the influential paper of Erian *et al.* [17], accounted for spatial effects and included linear and nonlinear laws for flow of maternal blood in the villous tissue described as a porous medium (the use of Darcy’s law in modelling maternal blood flow in the intervillous space is discussed in detail by Schmid-Schönbein [18]); other models have taken account of the radial oxygen diffusion at the scale of a single capillary in the intervillous space [19–21], and have considered blood flow and pressure in the spiral artery with a terminal expansion as a function of arterial radius using Poiseuille’s law for a conical tube [22]. A brief description, and main outcome, of each relevant model is summarised in Table 1.

A weakness of many previous models is that they either focus on metabolic exchange

but assume homogeneous maternal blood flow distribution through the placenta, or they describe complex flow of maternal blood but pay little attention to uptake kinetics and solute patterns. To address these combined effects, we present a theoretical model for maternal blood flow in a mature human placentone. We illustrate the qualitative effect of flow on solute uptake using representative simulations of transport of a nutrient that satisfies simple kinetics, without accounting at this stage for its transport in the fetal circulation. Our aim is to examine the influence of the decidual vessels' position and maternal blood flow rates on the flow and solute patterns in a single mature placentone in terms of key geometric and physical parameters.

2. The mathematical model

2.1. Outline

We model the villous tree in a placentone as an undeformable porous medium of uniform and isotropic hydraulic conductivity k . The intervillous space is perfused by an incompressible Newtonian liquid of viscosity μ , representing maternal blood. The placentone is assumed to be enclosed in an impermeable hemisphere (S_2), at the circular base of which (S_1) are a central source (a spiral artery), supplying blood with steady flow rate q , and two identical sinks (decidual veins), aligned along a diameter of the basal plate (see Fig. 2a). The radius L of the hemisphere characterises the size of the fetal villous tree; the sinks are placed symmetrically with respect to the source on S_1 a distance $\pm z_v$ from it, where $0 < z_v < L$. This three-dimensional geometry mimics the shape of the placentone (see Fig. 1). The placentone border is assumed impermeable, due to the presence of septa and adjacent placentones. We consider steady flow that is axisymmetric about the line through the source and sinks (Fig. 2a), ignoring pulsatile variations in flow from the spiral artery. Uterine contractions are also neglected due to the shorter timescales required for the perfusion of a placentone (< 1 min) compared to the period of relaxation (≈ 5 min) [2]. We also consider the situation in which the porous medium contains a central cavity above the spiral artery (Fig. 2b).

The advantage of assuming such a simple geometry for a placentone is that the transport problem can be solved analytically to obtain flow and pressure fields in an explicit form; the method and solution are outlined in full in the Supplementary Material. We also briefly illustrate the effect of flow on the distribution of a nutrient that is taken up into the villous tree.

The model assumes that the flow of maternal blood in the intervillous space is described by Darcy's law [23, 24]. This is a standard description of flow in a porous medium which

states that the average blood velocity is proportional to the local pressure gradient of maternal blood, the constant of proportionality being the hydraulic conductivity k divided by the effective blood viscosity μ . For a detailed discussion of the applicability of Darcy’s law in the present context see [17, 18]. Darcy’s equation enables the distribution of intervillous blood pressure P to be determined. The steady concentration C of a passive solute is described by an advection-reaction equation (see (B.1) in Supplementary Material), according to which the solute is convected along streamlines and “absorbed” by the solid phase of the porous medium under first-order kinetics at a rate αC , where α is a constant. The streamlines correspond to the average trajectories of fluid “particles” through the intervillous space. This type of uptake kinetics may be appropriate in the case of passive transport of certain metabolites, for which advective transport dominates over molecular diffusion; we do not seek to account explicitly for the more complex reaction kinetics of dissolved gases in maternal and fetal blood [7, 15]. Typical quantitative data for a normal placenta at term are presented in Table 2.

When the volume flux q of maternal blood into the placentone is prescribed, the problem is characterised by two dimensionless parameters: the uptake parameter (also known as the Damköhler number) $Da = \alpha L^3/q$, which expresses the local nutrient consumption rate in fetal terminal villi relative to the rate of convective mass transfer by maternal blood; and the geometrical ratio $h = z_v/L$ (where $0 < h < 1$), which reflects the position of the basal vessels relative to the placentone boundary.

The *absolute net uptake rate* N_a of a solute from the maternal blood is defined as the difference between the concentration flux at the source $q C_0$ and the concentration flux at the sinks. The *relative net uptake rate* (measured relative to the available flux of solute) is defined as $N_r = N_a/q C_0$ (see (B.4) in Supplementary Material). These integral measures enable us to investigate the influence of model parameters Da and h on the net uptake efficiency of the placentone.

If, instead of q , the difference in blood pressure ΔP between the supplying spiral artery and draining decidual veins is prescribed, we must evaluate q in terms of the hydraulic conductivity k of the porous medium, which depends on the volume fraction ϕ of space occupied by villous branches. Variation of the geometric parameters h and ϕ in the model enables us to explore how the placentone’s structure influences its function in terms of solute uptake.

2.2. Model limitations

The predictions of the model should be interpreted with some caution, being more qualitative than quantitative. The limitations of the model are rooted in its assumptions, which serve only as a first approximation to placentone anatomy and physiology.

For example, the human placentone's shape is not a perfect hemisphere; the central position of the spiral artery and only two draining veins per placentone symmetric about the centre are over-simplifications; the placentone is not completely isolated, and there is likely to be an interaction between adjacent placentones, especially in the central part of the human placenta; and the compliance, anisotropy and heterogeneity of the villous tissue are neglected.

The model does not account explicitly for the fetal placental circulation and neglects the inertia and pulsatility of entering maternal blood, as well as uterine contractions. Newtonian rheology is assumed for maternal blood flow in the intervillous space, ignoring the complexities involved in modelling the flow of a concentrated suspension of deformable cells in a porous medium.

Finally, the contribution of diffusion due to molecular motion and dispersion inside the intervillous space is not considered. The representative nutrient transported across the placentone is assumed to have homogeneous solubility, and facilitated or active transport factors are not explicitly accounted for. We focus therefore on uptake of passive inert substances into placental villous tissue, neglecting possible reversibility of materno-fetal solute exchange. Our model may be applicable to the case of low concentration of solute in the fetal circulation relative to its concentration in the intervillous space [14].

However, the advantage of assuming a simple structure and physiology of a placentone is that it allows for a mathematically transparent analysis of its function. This will, we hope, bring some insight to the development of more advanced models for placental circulation and metabolic exchange.

3. Results

3.1. Flow and pressure distributions

Fig. 3 shows flow and pressure fields in a hemispherical placentone with two different relative decidual artery-vein distances. Streamlines (blue, in Fig. 3(*a,b*)) display paths followed by maternal blood from the central spiral artery outwards to the two decidual veins. Because of the axial symmetry of flow (Fig. 2), the streamlines do not depend on the azimuthal angle θ . The orthogonal green isobars show how the pressure falls from a high value near

the flow source to a low value near each sink; the isobars meet the impermeable placentone boundaries orthogonally. The pressure distribution along the z -axis (Fig. 3(*c,d*)) shows how the pressure rises (falls) rapidly near the artery (veins), determining the overall pressure drop ΔP across the placenta. The intervillous pressure on the hemispherical boundary, far from these vessels, with a value intermediate between the arterial and venous pressures, is close to $P_{\text{ref}} = 5$ mmHg (see Supplementary Material for more details); the pressure drop ΔP across the placentone shown in Fig. 3(*c,d*) for the reference values of Table 2 is moderate, exhibiting low resistance to the maternal flow in the intervillous space [25]. The magnitudes of the pressures at the exit of the spiral artery and inlets of the decidual veins are primarily determined in the model by the width of the vessels and the volume fluxes passing through them.

When the distance between the source and sinks is small compared to the width of the placentone ($h = z_v/L = 0.45$, Fig. 3(*a,c*)), the flow pattern is localised due to the short-circuit of blood from the basal arteries to the nearby veins, unlike the flow that penetrates deeper into the dense intervillous space when the veins are situated near the periphery of the placentone (Fig. 3(*b,d*)). While flow patterns depend strongly on h , the overall conductivity of the placentone (the ratio of flow rate q to the overall pressure drop ΔP) is relatively insensitive to either the source-sink distance z_v or the placentone radius L , being instead approximately proportional to the ratio ka/μ , where a is a length comparable to the radius of the exit of the spiral artery and the entrance of each decidual vein, or whichever is the smaller (see Supplementary Material, equations (A.9) and (A.10)).

3.2. Tracer dynamics in the placentone

The early visualisation methods of the uteroplacental blood circulation by radioangiography were developed and applied to the primate and human uterus by Borell, Ramsey, Freese and others [1, 2, 26]. The method consists of an injection of a bolus of radio-opaque contrast medium into the systemic circulation and subsequent serial x-ray imaging of the uterus (typically, 60 – 70 ml of contrast medium is administered in about 5 sec [1, 26]; assuming the total blood supply of the placenta to be 500 ml/min (see Table 2), the filling time of the uterus with a bolus of radio-opaque material is of the order of 10 sec). Here we model the intensity distribution on radiographic images of a bolus of material as it enters the placentone and spreads outwards from the mouth of the spiral artery. We do this by tracking the axisymmetric surfaces at the leading and trailing edge of the bolus, and computing the distance between them in the direction perpendicular to the basal plate (the anterior-posterior direction of x-ray imaging of the placenta). Assuming the radio-opaque

material is distributed uniformly between the two surfaces, this distance will be proportional to the relative intensity of the resulting radioangiographic image.

Fig. 4(a) shows the leading and trailing fronts of tracer (blue dots) and the distance between them (solid red) in a section perpendicular to the basal plate at a fixed moment of time following the introduction of a passive tracer into the spiral artery; the time-dependence of cross-sectional area occupied by a tracer bolus is plotted in Fig. 4(d). The growth rate of the bolus area slows down as it approaches the veins at the periphery of the placentone.

Ring-like structures, colloquially (but inappropriately, given the absence of rotation of fluid particles) known as “smoke rings” [1, 7], appear on x-ray images of the primate and human uterus shortly after injection as shown in Fig. 4(e) by Freese [1]. We visualise the tracer distribution as explained above using two tracer fronts separated by a 10 sec time interval, projected to the basal plate in Fig. 4(b,c) ($h = 0.99$). The non-uniform intensity distribution arises because the thickness of the radially expanding bolus shell is maximal near its margins (Fig. 4a). The bright ring remains approximately circular until it gets close to the decidual veins (Fig. 4c).

3.3. Representative solute distributions

Representative solute concentration distributions at varying values of the non-dimensional uptake parameter $Da = \alpha L^3/q$ and varying artery-vein distances $h = z_v/L$ are depicted in Fig. 5. Fig. 5(a,b) show the effect of changing the artery-vein distance, and Fig. 5(c,d) show the effect of varying the local solute consumption rate α relative to the inlet volume flux q . The consequence of reducing the source-sink distance is similar to increasing the uptake parameter Da ; in both Fig. 5(a) and Fig. 5(d) the nutrient pattern is localised towards the basal half of the placentone. Comparing Figures 5(b) and 5(c), we see that the solute concentration near the veins is increased (in Fig. 5c) by reducing Da , i.e. by reducing the local consumption rate α , the size of the placentone L or by increasing the inlet flow rate q , effects which reduce the overall relative net uptake rate N_r . Additional computations indicate that N_r increases if the veins are located towards the periphery of the placentone (see Fig. S1(a) in Supplementary Material). The dependence of net uptake rate on inlet flow rate is more subtle: computations show that N_a/q_0C_0 , the ratio of the absolute net uptake rate to a fixed inlet solute flux q_0C_0 , increases with q (Figs 5(d), 5(b), 5(c) illustrate an increase in q), as more material is delivered to the placentone per unit time by the increased flux; measured relative to the increasing flux of available solute qC_0 , however, the relative net uptake rate $N_r = N_a/qC_0$ falls with q , as there is less time available for absorption to take place at higher flow rates as nutrient passes through the placentone more rapidly. At high blood flow

speeds (Fig. 5c) the concentration distribution in the hemisphere is nearly equal to the initial solute concentration in the spiral artery, making the solute consumption rate α a limiting factor for solute extraction.

3.4. Influence of the central cavity

In order to investigate the role of the central cavity of the placentone in the framework of our mathematical model, we employ the following additional assumptions: first, the solute consumption rate in the central cavity is zero; second, the border of the central cavity is delineated by a constant pressure line of the flow in a homogeneous hemisphere (one of the isobars shown in green in Fig. 3b). The latter condition corresponds to the case when the flow velocity of maternal blood in the dense intervillous space is slow relative to the blood motion in the central cavity, allowing the pressure to equilibrate within the cavity.

The effect of varying the size of the central cavity is shown in Fig. 6(a,b), where flow and concentration distributions are presented for a small and large cavity. We define the effective cavity radius R as the square root of its cross-sectional area A ($R = \sqrt{2A/\pi}$); the pressure drop ΔP between the central cavity and the decidual veins is held constant in the two simulations.

The large cavity leads to a “boundary-layer”-like solute distribution pattern in the intervillous space with higher concentrations in the upper half of the domain (Fig. 6b) compared to the case of homogeneous uptake in the placentone (Fig. 5b). This follows from the assumption that blood is driven by the same pressure drop (between the central cavity and the decidual veins) toward the top and the side of the placentone, and therefore the flow velocities in the top region are smaller than velocities in the lower part. The relative net uptake rate N_r decreases with increasing cavity size at constant pressure drop (see Fig. 6(b)). The smaller volume of villous tissue provides less flow resistance, so that q increases with R ; at the same time, the smaller volume has less capacity to absorb nutrient. Both effects cause N_r to fall with R . However, computations show that the dependence of the absolute net uptake rate N_a (relative to the reference concentration flux $q_0 C_0$) on the cavity radius exhibits a peak for an intermediate cavity size, indicating an optimal relation between the resistance to maternal blood perfusion and the amount of villous tissue participating in solute uptake (see Fig. S2(b) in Supplementary Material). While uptake is low for large R , the cavity may play an important role in shielding villous tissue from harmful shear stresses associated with maternal blood emerging from the spiral artery.

4. Discussion

We have developed a mathematical model to describe steady maternal flow and solute transport in the human placentone. The placenta is characterised by high degrees of geometric complexity and substantial variability between individuals. We have sought to incorporate only the most significant geometric and haemodynamical features in our model of intervillous blood flow, treating the placentone as a hemispherical structure (Fig. 2). This enabled us to derive an analytical expression for the three-dimensional internal flow field (see Equation (A.7) in Supplementary Material), from which simple estimates of nutrient uptake were obtained. Bearing all these limitations in mind, we can now assess the model's predictions.

First, in the absence of a cavity, the localised source and sinks that drive flow through the villous tree (Fig. 3) show large flow speeds (about 2 cm/s at a distance of order 1 mm from the spiral artery for parameter values from Table 2, shown by crowding of streamlines, which is broadly consistent with estimates of Burton *et al.* [22]) and large pressure gradients in the immediate neighbourhood of the decidual artery and veins. This implies that shear stresses on villous tissue will be largest in these locations. These flow patterns provide a strong argument for the remodelling of the tree to form a cavity above the arterial opening (Fig. 6), and possibly above the veins also, to protect tissues from high stresses [27] and to increase the overall conductance of the placentone. Our model also shows that, in a homogeneous placentone, intervillous flow is more evenly distributed when the decidual veins are located peripherally (see Fig. S1(a) in Supplementary Material), supporting the hypothesis [8, 9] that decidual veins are primarily located at the periphery of the placentone. It may be possible to generalise these findings to explain potential benefits arising from elevated openings of decidual veins on the placental septa [7, 28].

Our model indicates that the calibre of the spiral artery and decidual veins may be a dominant determinant of the overall conductance of the placentone. In particular, Equation (A.9) of Supplementary Material shows that the ratio of the maternal blood flow rate q through the placentone to the driving pressure difference ΔP between the spiral artery and decidual veins is $4\pi ka/3\mu$, where k is the effective hydraulic conductivity of the villous tissue, μ is the effective viscosity of maternal blood and a is a lengthscale representative of the calibre of the spiral artery and decidual veins where they meet the basal plate of placenta. This may have implications for placental insufficiency such as in pre-eclampsia, where inadequate trophoblast invasion of spiral arteries may result in reduced luminal diameter [22] and hence significantly reduced placentone conductance to maternal blood flow. In case of an early onset

of failed trophoblast invasion leading to lower arterial calibre a over normal values, there may be sufficient time available for compensatory remodelling of the villous tree (increasing the placentone conductivity k) to maintain physiologically normal values of q at constant pressure drop ΔP . However, if the dilation of spiral arteries is impaired in the late stage of pregnancy, or an acute constriction of the supplying vessels takes place, there may not be sufficient time for compensatory remodelling of the villous tree; here k would remain constant, and maternal systemic arterial blood pressure would have to be elevated in order to maintain the same flow rate level q at the reduced value of a . It would be of interest to verify experimentally the linear dependence (predicted in Equation (A.9)) of maternal blood flow rate through an isolated fetal cotyledon on the calibre of the cannula used to mimic the spiral artery in an *ex vivo* perfusion model.

The model predictions of tracer distribution in a placentone (see Fig. 4) are in accord with radioangiographic observations *in vivo* in primates and humans. The formation of a ring-like structure growing with time is demonstrated even without explicitly accounting for a central cavity in the placentone. We hope that rapid development of new techniques in ultrasound imaging [29, 30], complementing traditional radioangiography and used in conjunction with mathematical modelling, may offer new tools for monitoring placental function with a lower risk to mother and fetus.

Given the essential physiological role of the placenta in gas and nutrient transfer, we also provided simulations of uptake of a representative solute into the villous tree in order to illustrate flow properties. For a given geometry, the ratio of nutrient uptake rate to volume flux, expressed by the dimensionless Damköhler number $Da = \alpha L^3/q$, determines the homogeneity of uptake: if Da is sufficiently large, for example, uptake is confined to the immediate neighbourhood of the spiral artery (Fig. 5*d*). Evidently materials with differing uptake rates and kinetics (and therefore different Da) will be absorbed in different regions of the placentone. The relative net uptake rate N_r can be interpreted as a relative difference between solute concentrations in the spiral artery and decidual vein, scaled with arterial concentration at constant blood flow rate in the spiral artery. A range of values for oxygen partial pressure suggests that N_r for oxygen varies between 0.3 and 0.7 [16], which is close to the predicted range (shown in Fig. S1(*a*), Supplementary Material).

The placentone exhibits a trade-off between flow resistance and uptake capacity. A higher density of villous material offers a larger surface area for uptake, but also higher flow resistance and hence lower perfusion (for a given pressure drop between artery and veins). Likewise with a low density of villous tissue, nutrients could flow rapidly through the pla-

centone, too quickly for substantial uptake to take place. An important characteristic of the placentone is the volume fraction of villous tissue ϕ (the ratio of the volume occupied by villi to the total volume of the placentone). We used our model to demonstrate the existence of an optimal volume fraction of $\phi \approx 0.3$ that maximises the absolute net uptake rate of our representative solute (see Fig. S2(a) in Supplementary Material). Estimates of the villous volume fraction, based on stereological data of Mayhew [31] for normal, high-altitude and diabetic placentas, vary between approximately 0.3 and 0.6 with a tendency towards low values in the high-altitude group, used as a model for pre-eclampsia; there was no significant difference in the volume of intervillous space and villous volume between the control and diabetic groups [31]. Numerous additional factors will influence the optimal value of ϕ , which we did not explore explicitly here. We emphasise again that the predictions of the model are of more qualitative than quantitative accuracy.

Future models will need to address the implications of assuming an idealised geometry and our numerous other approximations (see Sec. 2.2). For instance, while the rheology of blood in narrow capillaries has been well characterised experimentally [32], little is known at present about the rheology of maternal blood moving through tortuous intervillous spaces. We also ignored the inertia and pulsatility of a jet of maternal blood issuing from a spiral artery. These factors will be attenuated both by mixing in the cavity above the artery and by viscous effects in the intervillous space: while the Reynolds number based on placentone diameter is of order unity (Table 2), the Reynolds number based on intervillous pore diameter is substantially smaller, and so inertial effects can safely be neglected everywhere except possibly in the immediate neighbourhood of the spiral artery [22]. We have taken no account of the deformability of the villous tissue, and spatial non-uniformity in material properties was accounted for only by assuming the presence of a cavity above the spiral artery. We have also considered only very simple models of advective nutrient transport and uptake, neglecting diffusion relative to advection, ignoring transport in the fetal microcirculation and assuming only simple uptake kinetics.

A priority for future theoretical studies is to account explicitly for the micro-architecture of the villous tree to give improved estimates of hydraulic conductivity and uptake as a function of volume fraction. These can then be used to assess with more confidence the relation between the structure and function of the placentone in health and disease. Likewise, models can be extended to identify the optimal cavity size, trading increased conductance and protection from elevated shear stresses and oxygen tension [28] against reduced uptake efficiency.

Acknowledgements

The authors are grateful to Dr. Matthew Finn for his important contributions to the early stages of this study. We also would like to thank Professor Graham Burton, University of Cambridge, for his interest to the work and helpful comments on the draft of this manuscript. The work is supported by the Marie Curie Network MMBNOTT (Project No. MEST-CT-2005-020723).

References

- [1] Freese UE. The uteroplacental vascular relationship in the human. *Am J Obstet Gynecol* 1968; 101:8–16.
- [2] Ramsey EM. Uteroplacental circulation during labor. *Clin Obstet Gynecol* 1968; 11:78–95.
- [3] Reynolds SRM. Derivation of the vascular elements in the fetal cotyledon of the hemochorial placenta: A contribution to the theory of placental morphogenesis. *Anat Rec* 1967; 157:43–46.
- [4] Wilkin P. Contribution to the study of the fetal placental circulation. *Gynécologie et Obstétrique* 1954; 53:239–263, (in French).
- [5] Wigglesworth JS. Vascular organization of the human placenta. *Nature* 1967; 216:1120–1121.
- [6] Schuhmann RA. Placentone structure of the human placenta. In *Structural and Functional Organization of the Placenta*, (Eds.) Kaufmann P and King B, no. 22 in *Bibliotheca Anatomica*, Karger 1982; pp. 46–57.
- [7] Benirschke K, Kaufmann P and Baergen RN. *Pathology of the Human Placenta*. Springer, 5th ed. 2006, 1050 pp.
- [8] Freese UE. Vascular relations of placental exchange areas in primates and man. In *Respiratory gas exchange and blood flow in the placenta*, (Eds.) Longo LD and Bartels H, Bethesda, Md.: Nat. Inst. Child Health Hum. Dev. 1972; pp. 31–60.
- [9] Boyd JD and Hamilton WJ. *The Human Placenta*. Cambridge: W.Heffer&Sons Ltd. 1970, 365 pp.

- [10] Schröder HJ. Comparative aspects of placental exchange functions. *Eur J Obstet Gynecol Reprod Biol* 1995; 63:81–90.
- [11] Kirschbaum TH and Shapiro NZ. A mathematical model of placental oxygen transfer. *J Theor Biol* 1969; 25:380–402.
- [12] Faber JJ. Application of the theory of heat exchangers to the transfer of inert materials in placentas. *Circ Res* 1969; 24:221–234.
- [13] Longo LD and Bartels H (eds.), *Respiratory Gas Exchange and Blood Flow in the Placenta*, Bethesda, Md.: Nat. Inst. Child Health Hum. Dev. 1972, p. 570.
- [14] Bartels H and Moll W. Passage of inert substances and oxygen in the human placenta. *Pflügers Arch Eur J Physiol* 1964; 280:165–177.
- [15] Hill E, Power G and Longo L. A mathematical model of carbon dioxide transfer in the placenta and its interaction with oxygen. *Am J Physiol* 1973; 224:283–299.
- [16] Lardner TJ. A model for placental oxygen exchange. *J Biomech* 1975; 8:131–134.
- [17] Erian FF, Corrsin S and Davis SH. Maternal, placental blood flow: A model with velocity-dependent permeability. *J Biomech* 1977; 10:807–814.
- [18] Schmid-Schönbein H. Conceptual proposition for a specific microcirculatory problem: maternal blood flow in hemochorial multivillous placentae as percolation of a “porous medium”. *Trophoblast Res* 1988; 3:17–38.
- [19] Guilbeau EJ, Reneau DD and Knisely MH. The effects of placental oxygen consumption and the contractions of labor on fetal oxygen supply: A steady and unsteady state mathematical simulation. In *Respiratory Gas Exchange and Blood Flow in the Placenta*, (Eds.) Longo LD and Bartels H, Bethesda, Md.: Nat. Inst. Child Health Hum. Dev. 1972; pp. 297–342.
- [20] Heilmann L, Grebner H, Mattheck C and Ludwig H. Mathematical, clinical, and laboratory study of hemodynamic changes in the placental circulation. *Arch Gynecol Obstet* 1979; 227:303–313.
- [21] Costa A, Costantino M and Fumero R. Oxygen exchange mechanisms in the human placenta: mathematical modelling and simulation. *J Biomed Eng* 1992; 14:385–389.

- [22] Burton G, Woods A, Jauniaux E and Kingdom J. Rheological and physiological consequences of conversion of the maternal spiral arteries for uteroplacental blood flow during human pregnancy. *Placenta* 2009; 30:473–482.
- [23] Bear J. *Dynamics of Fluids in Porous Media*. Dover Publications 1988, 784 pp.
- [24] Batchelor GK. *An Introduction to Fluid Dynamics*. Cambridge Math. Lib., Cambridge Univ. Press 2000, 635 pp.
- [25] Moll W, Wallenburg HCS, Kastendieck E and Voslar M. The flow resistance of the spiral artery and the related intervillous space in the rhesus monkey placenta. *Pflügers Arch Eur J Physiol* 1978; 377:225–228.
- [26] Borell U, Fernström I, Ohlson L and Wiqvist N. An arteriographic study of the blood flow through the uterus and the placenta at midpregnancy. *Acta Obstet Gynecol Scand* 1965; 44:22–31.
- [27] Soghomonians A, Barakat AI, Thirkill TL, Blankenship TN and Douglas GC. Effect of shear stress on migration and integrin expression in macaque trophoblast cells. *Biochim Biophys Acta - Mol Cell Res* 2002; 1589:233–246.
- [28] Hempstock J, Bao YP, Bar-Issac M, Segaren N, Watson AL, Charnock-Jones DS, Jauniaux E and Burton GJ. Intralobular differences in antioxidant enzyme expression and activity reflect the pattern of maternal arterial bloodflow within the human placenta. *Placenta* 2003; 24:517–523.
- [29] Konje JC, Huppertz B, Bell SC, Taylor DJ and Kaufmann P. 3-dimensional colour power angiography for staging human placental development. *The Lancet* 2003; 362:1199–1201.
- [30] Abramowicz J and Sheiner E. Ultrasound of the placenta: A systematic approach. Part II: Functional assessment (Doppler). *Placenta* 2008; 29:921–929.
- [31] Mayhew TM. Patterns of villous and intervillous space growth in human placentas from normal and abnormal pregnancies. *Eur J Obstet Gynecol Reprod Biol* 1996; 68:75–82.
- [32] Popel AS and Johnson PC. Microcirculation and hemorheology. *Annu Rev Fluid Mech* 2005; 37:43–69.
- [33] Aifantis EC. Towards a rational modeling for the human placenta. *Math Biosci* 1978; 40:281–301.

- [34] Wilbur WJ, Power GG and Longo LD. Water exchange in the placenta: a mathematical model. *Am J Physiol Regul Integr Comp Physiol* 1978; 235:R181–199.
- [35] Schröder H. Fluid shift across the placenta: III. Application of a computer model of passive placental transfer. *Placenta* 1982; 3:349–357.
- [36] Groome LJ. A theoretical analysis of the effect of placental metabolism on fetal oxygenation under conditions of limited oxygen availability. *Biosystems* 1991; 26:45–56.
- [37] Banerjee RK, Kwon O, Vaidya VS and Back LH. Coupled oxygen transport analysis in the avascular wall of a coronary artery stenosis during angioplasty. *J Biomech* 2008; 41:475–479.
- [38] Roos MW and Sperber GO. A diffusion model of cerebral microischemia. *Exp Neurol* 1997; 147:142–150.
- [39] Prendergast CH, Parker KH, Gray R, Venkatesan S, Bannister P, Castro-Soares J, Murphy KW, Beard RW, Regan L, Robinson S, Steer P, Halliday D and Johnston DG. Glucose production by the human placenta in vivo. *Placenta* 1999; 20:591–598.
- [40] Espinoza J, Romero R, Mee Kim Y, Kusanovic JP, Hassan S, Erez O, Gotsch F, Gabor Than N, Papp Z and Jai Kim C. Normal and abnormal transformation of the spiral arteries during pregnancy. *J Perinat Med* 2006; 34:447–458.
- [41] Moore KL and Persaud TVN. *The Developing Human : Clinically Oriented Embryology*. Philadelphia: Saunders, 7th ed. 2003, 560 pp.
- [42] Milne-Thomson LM. *Theoretical Hydrodynamics*. New York: Macmillan, 5th ed. 1968, 743 pp.

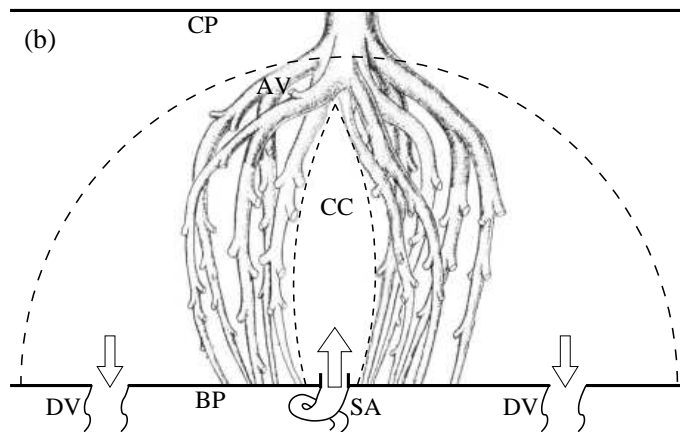
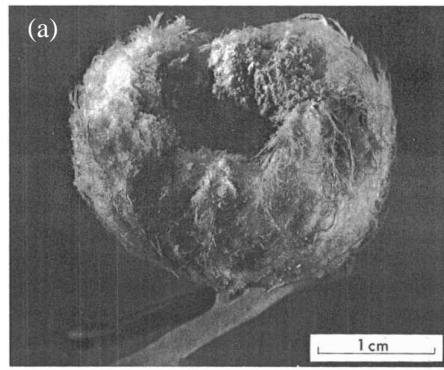


Figure 1. (a) A cast of a large villous tree from the human term placenta (incomplete injection, reproduced from [8] with permission), showing differences in density of villi forming a central cavity (top). (b) A schematic (modified from [7]) of the placentone at term, enclosed between the basal (BP) and chorionic (CP) plates. Maternal blood enters the central cavity (CC) via the spiral artery (SA) and is drained through the decidual veins (DV) at the periphery. Note the anchoring stem villi (AV) surrounding the CC and connecting the CP with the BP. The dashed lines show the central cavity and notional outer boundary of the placentone. The intermediate and terminal villi are not shown.

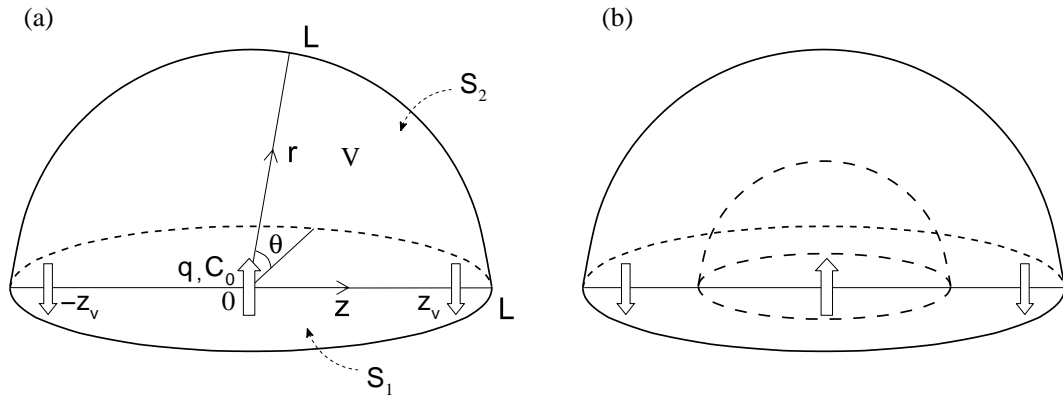


Figure 2. A schematic placental circulatory unit confined between the plane S_1 and hemispherical surface S_2 of radius L . Maternal blood enters from a source (artery) at $z = 0$ and exits through sinks (veins) at $z = \pm z_v$, as indicated by arrows: (a) a homogeneous intervillous space; (b) including a central cavity. In the cylindrical coordinate system, z measures distance along the axis in S_1 on which the spiral artery and decidual veins lie; r measures distance perpendicular to this axis. The flow is assumed axisymmetric, i.e. independent of the azimuthal angle θ measured in a plane perpendicular to the z -axis from the plane S_1 .

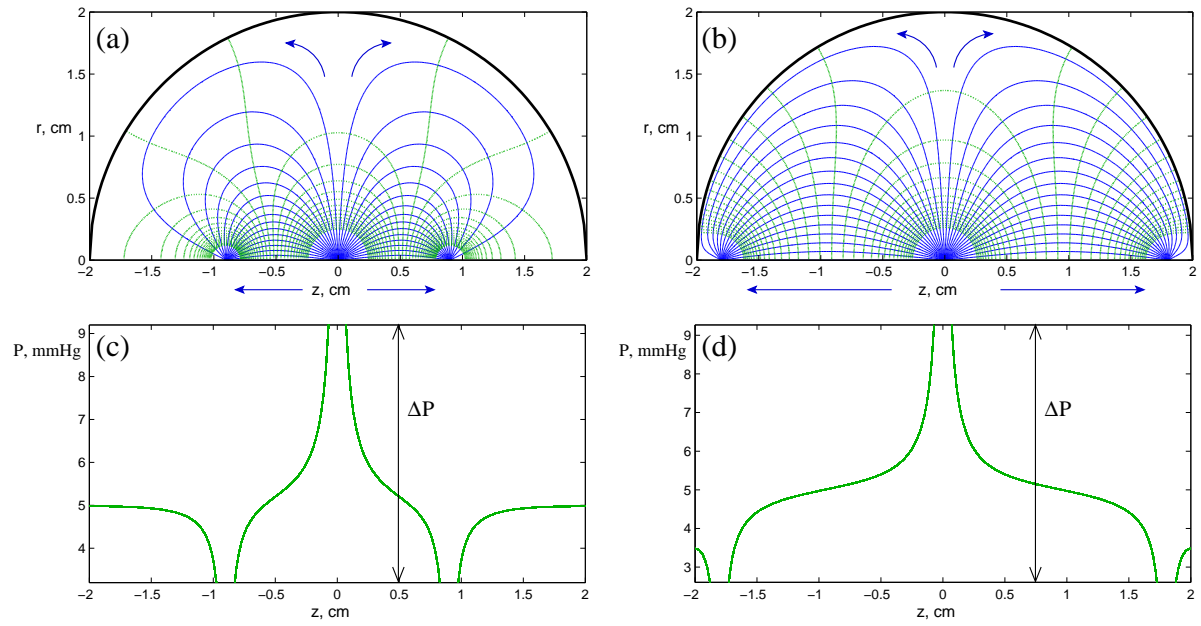


Figure 3. (a,b) predicted streamlines (blue) and constant pressure lines (green) for steady flow in a homogeneous placentone plotted in a cross-section perpendicular to the z -axis holding the basal vessels, where r is a distance from the axis of symmetry. Arrows indicate the direction of flow. (c,d) Intervillous blood pressure along the z -axis ($r \simeq 0.005$ cm, $P_{ref} = 5$ mmHg, $q_0 = 5$ ml/min). The decidual veins are located either near the centre ((a,c), $h = 0.45$) or near the periphery ((b,d), $h = 0.9$) of the placentone.

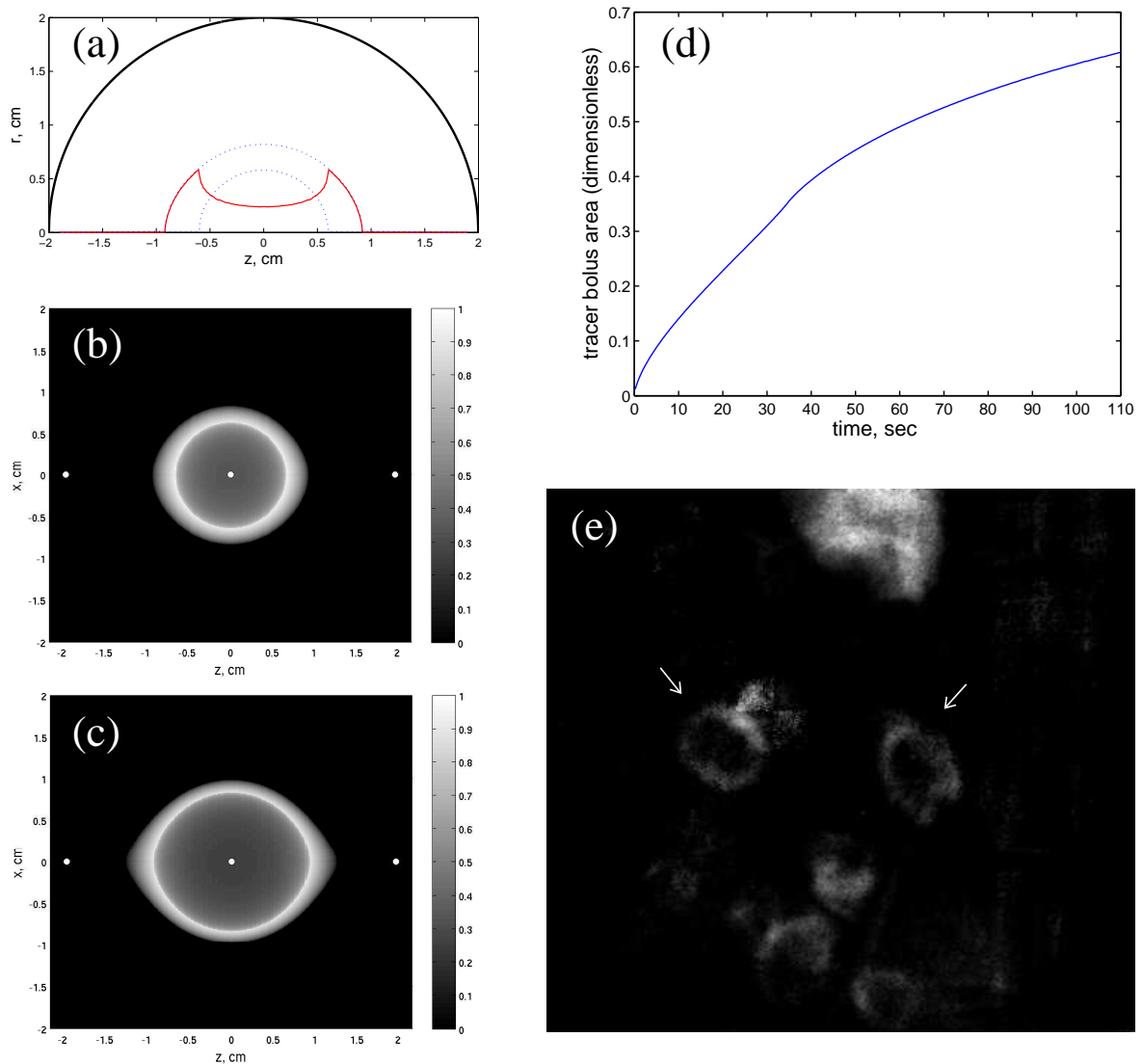


Figure 4. Tracer dynamics in the placentone: (a) leading and trailing tracer fronts (blue dots) and the shell thickness profile (solid red, representing x-ray intensity) 15 sec following the appearance of the tracer from the spiral artery (shown in a sagittal section through the placentone; the decidual veins lie at $z \simeq \pm 2$ cm); (b,c) computed intensity of the tracer (grayscale) in the orthogonal projection on the basal plate 15 sec (b) and 25 sec (c) after the introduction of tracer to the model (white dots indicate the location of the spiral artery and decidual veins); (d) dependence of cross-sectional area of tracer bolus on time; (e) serial radioangiographic film of monkey uterus 18.5 sec following injection of Renografin (arrows indicate ring-like structures), reproduced from [1].

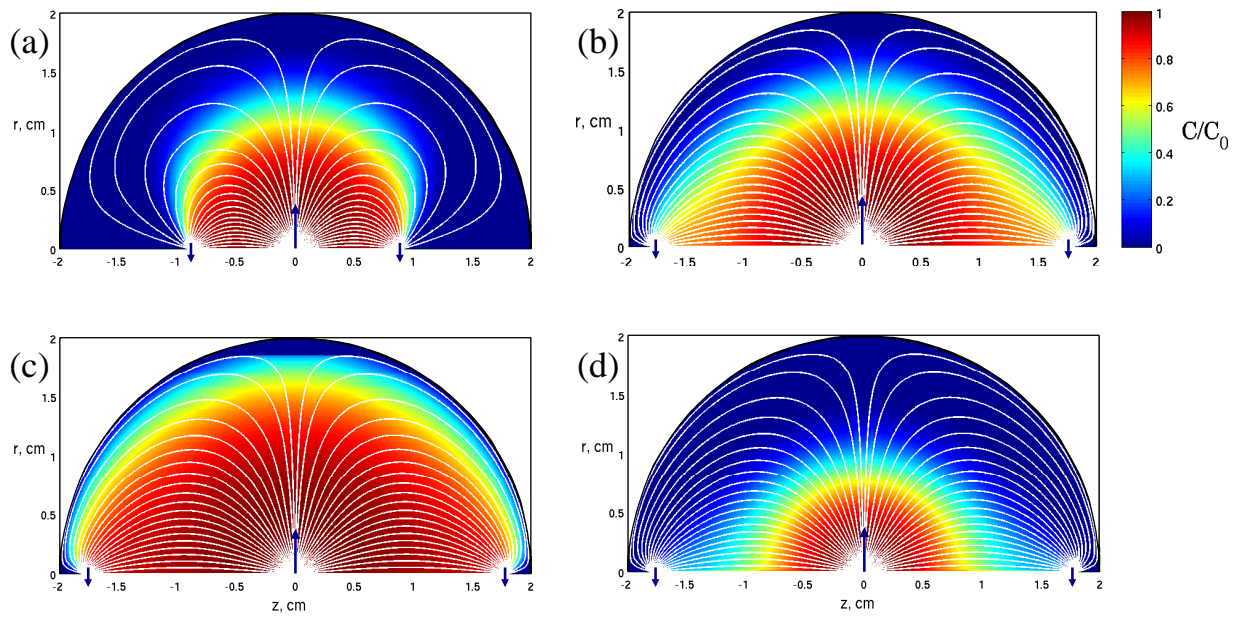


Figure 5. Streamlines (white lines) and normalised concentration field (C/C_0 , colours) in the placentone for different values of uptake parameter and relative position of the decidual veins (arrows): (a) small source-sink distance ($Da = 1$, $h = 0.45$); (b) veins near the periphery ($Da = 1$, $h = 0.9$); (c) low uptake rate ($Da = 0.25$, $h = 0.9$); (d) high uptake rate ($Da = 4$, $h = 0.9$). The corresponding values of the relative net uptake rate N_r are (a) 0.43, (b) 0.68, (c) 0.33, (d) 0.94, and of the absolute net uptake rate N_a/q_0C_0 are (a) 0.43, (b) 0.68, (c) 1.34, (d) 0.24.

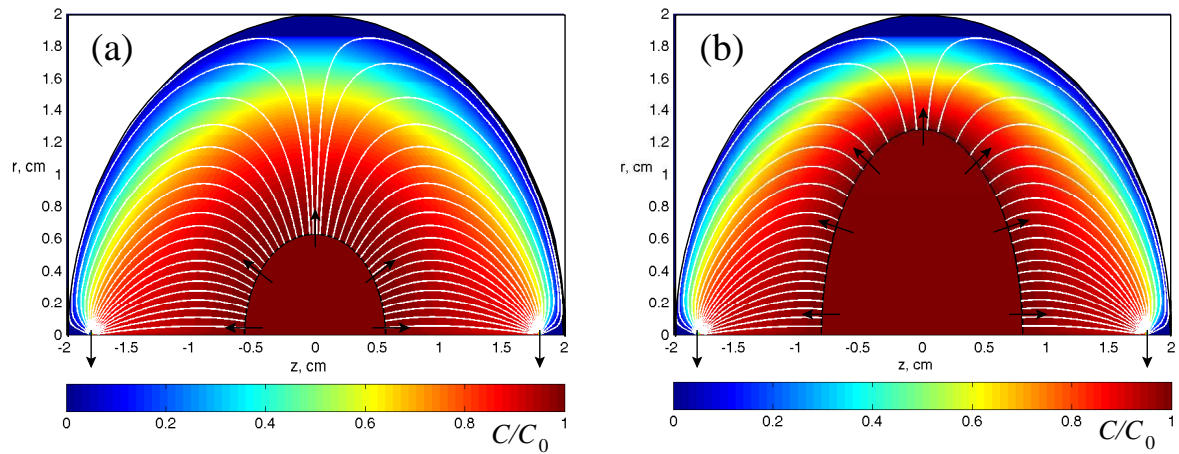


Figure 6. Flow streamlines (white lines) and concentration distribution (colours) in a hemisphere in the presence of the central cavity (assuming first-order uptake kinetics, $h = 0.9$): (a) a small cavity of effective radius $R \simeq 0.6$ cm with $Da \simeq 0.43$ outside the cavity and relative net uptake rate $N_r \simeq 0.45$; (b) a large cavity of effective radius $R \simeq 1$ cm with $Da \simeq 0.39$ and $N_r \simeq 0.37$.

Model	Description	Main results
Kirschbaum, Shapiro (1969) [11]	Equilibrium mass transfer in the lamb placenta. A system of algebraic equations is derived from Fick's law for diffusion and Hill's law for uptake.	The influence of the placental shunts is investigated. The distribution of blood flow-rate-fraction participating in materno-fetal gas exchange is presented.
Faber (1969) [12]	Steady transfer of inert solutes is considered for concurrent, countercurrent, crosscurrent and "pool flow" arrangements of placental circulation based on a one-dimensional advection-mass transfer model. The effectiveness of solute transport with respect to the placental type and model parameters is analysed.	Three dimensionless parameters representing placental permeability, materno-fetal blood flow rates and solute transport rates are identified. The isolines of solute transport rates are plotted for homogeneous and heterogeneous blood flows and placental barrier permeability.
Guilbeau, Reneau, Knisely (1972) [19]	Steady and unsteady oxygen transfer in a capillary-scale unit of the human placenta, which is described by a system of diffusion-convection-reaction equations in a three-layer cylinder, with the Hill equation for oxygen saturation; placental shunts are neglected.	Spatio-temporal distributions of oxygen partial pressure in maternal and fetal blood near the exchange unit are computed. The effect of time-varying velocity of maternal blood on oxygen content is explored.
Hill, Power, Longo (1973) [15]	Unsteady gas transfer in the human placenta. A system of ODEs is obtained based on Fick's law in terms of O_2 and CO_2 partial pressures, using exponential and Hill-type dissociation kinetics in red blood cells.	The time course of O_2 and CO_2 partial pressures in the maternal and fetal erythrocytes and in plasma is obtained. The influence of kinetic parameters on transient processes is studied.
Lardner (1975) [16]	Steady one dimensional oxygen transfer in the human placenta. The model is described by a system of nonlinear ODEs, with combined linear and Hill-type uptake kinetics.	A set of dimensionless parameters characterising diffusion, uptake and flow rates is proposed. The dependence of oxygen uptake and partial pressure on these parameters is given.
Erian, Corrsin, Davis (1977) [17]	Steady maternal blood flow in a single placentone of the human placenta. Darcy's law with constant, spatially non-uniform and local maternal flow-velocity-dependent hydraulic conductivity is used.	The effect of villous distortion due to maternal blood flow on flow patterns is studied. A short-circuiting of maternal blood entering the placentone is predicted.
Aifantis (1978) [33]	A general scheme of haemodynamics and heat transfer in the human placenta, based on mixture theory.	A critical review of existing models is presented. A plan of future developments is proposed.

Table 1. Mathematical models proposed for the uteroplacental blood flow and solute transport. (ODEs = Ordinary differential equations).

Model	Description	Main results
Wilbur, Power, Longo (1978) [34]	Unsteady water and solute exchange in the human placenta as a generalisation of [15]. The model is given by a system of 36 ODEs, taking account of hydrostatic and osmotic pressures as well as chemical reactions for a variety of solutes.	Steady distribution of water and solute transfer rates between mother and fetus along placental membrane is given. Reversed exchange near the end of a fetal capillary is observed. A sensitivity analysis to the model parameters is performed.
Heilmann, Grebner, Mattheck, Ludwig (1979) [20]	Unsteady radial oxygen diffusion in a human placenta, described as two-layer Krogh cylinder with different diffusion coefficients for the blood-filled intervillous space and trophoblastic tissue; no oxygen uptake and zero maternal blood flow are assumed.	The model studies the rheological effect of a sudden occlusion in the intervillous space, caused by erythrocyte aggregation. The typical time of a physiologically significant decay in oxygen partial pressure is given.
Schröder (1982) [35]	Unsteady passive transport of solutes in the guinea-pig placenta. A one-dimensional mathematical model uses a generalisation of Fick's law to take account of hydrostatic and colloid osmotic pressure differences across a placental membrane at constant arterial flow rates.	Steady distributions of concentrations, hydrostatic and osmotic pressure along a placental membrane are obtained for both concurrent and counter-current flows. The computed osmotic pressure effect on transplacental bulk water exchange is compared with experimental data.
Schmid-Schönbein (1988) [18]	A schematic analysis of steady flow of maternal blood in the intervillous space as a porous medium is presented. Poiseuille and Darcy flows are compared and contrasted, using algebraic relations and the empirical Kozeny-Carman formula for placental hydraulic conductivity.	Experimental techniques to identify the parameters are proposed. An explanation of x-ray images of radio-opaque tracer as "percolating chromatographic fronts" is given. The role of non-Newtonian blood rheology at small flow velocities is highlighted.
Groome (1991) [36]	Steady one-dimensional oxygen transport in the human placenta, described by a system of nonlinear ODEs with a Hill-type law for haemoglobin dissociation, and Michaelis-Menten kinetics for uptake by syncytiotrophoblasts.	The effect of placental oxygen consumption, due to metabolism, on the fetal oxygenation in a microscopic uteroplacental unit is investigated. Placental vascular shunts are taken into account.
Costa, Constantino, Fumero (1992) [21]	Steady oxygen exchange in the human placenta, based on one-dimensional diffusion and uptake in an individual fetal capillary. Anatomical capillary network data is employed.	The dependence of oxygen partial pressure in fetal blood on gestational age and on thickness of the materno-fetal barrier is calculated.

Table 1. (continued).

Parameter	Value	Reference
Diameter of terminal villi (d)	$\simeq 50 \mu\text{m}$	[7]
Diffusivity in blood plasma (D) for oxygen glucose	$\simeq 10^{-3} \text{ cm}^2/\text{min}$	[37]
	$\simeq 10^{-4} \text{ cm}^2/\text{min}$	[38]
Arterial concentration (C_0) of dissolved oxygen glucose	$\simeq 0.1 \text{ mM}$	[15]
	$\simeq 4 \text{ mM}$	[39]
Radius of the decidual vessels (a)	$\simeq 1 \text{ mm}$	[40]
Number of basal arterial openings at term	$\simeq 100$	[7, 9]
Number of decidual vein outlets	50 – 200	[7]
Total flow rate of incoming blood	500 – 700 ml/min	[39, 41]
Flow rate per a single spiral artery (q_0)	5 ml/min	
Reference radius of a placentone (L_0)	2 cm	
Characteristic pressure drop in placentone (P_0)	$\sim 1 \text{ mmHg}$	
Reference blood pressure in placentone (P_{ref})	5 mmHg	
Reference solute consumption rate (α_0)	1 min^{-1}	
Placental hydraulic conductivity (k)	$\simeq 10^{-10} \text{ m}^2$	
Blood viscosity (μ)	$4 \times 10^{-3} \text{ Pa} \cdot \text{s}$	
Blood density (ρ)	10^3 kg/m^3	
Reynolds number ($Re = \rho q_0 / \mu L_0$)	~ 1	
Péclet number ($Pe = q_0 / L_0 D$)	$\sim 10^3 - 10^4$	

Table 2. Literature-based and calculated parameters for a normal full-term human placenta used in the model (all data for haemodynamics refer to the materno-placental/systemic circulation).

A mathematical model of intervillous blood flow in the human placentone

Igor L. Chernyavsky, Oliver E. Jensen, Lopa Leach

Supplementary Material

A. The method of images for Darcy's flow in a hemispherical domain

We use cylindrical coordinates (z, r, θ) with a local maternal blood velocity $\mathbf{u}(r, z) = (u_z(r, z), u_r(r, z), 0)$ to describe the axisymmetric flow, where z is the axis of symmetry (on which the source and sinks lie), r is the radial distance normal to the axis and θ is the azimuthal angle (so that the placentone occupies $|z| \leq L$, $0 \leq r \leq L$, $0 \leq \theta \leq \pi$, $r^2 + z^2 \leq L^2$, see Fig. 2a).

Neglecting fluid inertia due to the low Reynolds number (see Table 2) and averaging mass and momentum conservation laws over lengthscales large compared to the scale of villous microstructure, but small compared to the placentone radius L , we can describe the steady flow of maternal blood by Darcy's law [23, 24]

$$\nabla \cdot \mathbf{u} = 0, \quad (\text{A.1})$$

$$\mathbf{u} = -\frac{k}{\mu} \nabla P, \quad (\text{A.2})$$

where \mathbf{u} and P are the velocity and pressure of blood in the intervillous space; k is the hydraulic conductivity coefficient (inverse flow resistance) and μ is blood viscosity, which are both assumed constant.

Because Darcy flow (A.2) is by definition irrotational ($\nabla \times \mathbf{u} = 0$), we introduce a Stokes stream function and velocity potential with appropriate boundary conditions and apply the method of images to obtain the exact solution to the flow problem. In doing so we find analytical expressions for the pressure and velocity fields in closed form.

Equations (A.1)–(A.2) are solved subject to boundary conditions $\lim_{r \rightarrow 0} r u_r = \frac{q}{\pi} (\delta(z) - \frac{1}{2} [\delta(z - z_v) + \delta(z + z_v)])$ on $S_1 = \{r^2 + z^2 \leq L^2, \theta = 0, \theta = \pi\}$ and $\mathbf{u} \cdot \mathbf{n} = 0$ on $S_2 = \{r^2 + z^2 = L^2, 0 \leq \theta \leq \pi\}$; here the Dirac δ -function is used to approximate the flow rate distribution of a singular source and sinks, q is the flow rate at the source (which is split

equally between the sinks), and \mathbf{n} is the outward unit normal vector to the hemispherical surface S_2 . We explain how the finite sizes of the source and sink vessels influence the flow solution below.

The incompressibility condition (A.1) is identically satisfied if we introduce the Stokes stream function $\psi(r, z)$ in a cylindrical coordinate system, defined as $u_r = -\frac{1}{r} \frac{\partial \psi}{\partial z}$, $u_z = \frac{1}{r} \frac{\partial \psi}{\partial r}$, where u_r and u_z are radial and axial velocity components. We also introduce a velocity potential $\varphi = -\frac{k}{\mu} P$, such that $\mathbf{u} = \nabla \varphi$. Thus, from (A.1)–(A.2) we obtain

$$\nabla^2 \psi - \frac{2}{r} \frac{\partial \psi}{\partial r} = 0, \quad \nabla^2 P = 0, \quad (\text{A.3})$$

where $\nabla^2 \equiv (\nabla \cdot \nabla) = \partial^2 / \partial r^2 + r^{-1} \partial / \partial r + \partial^2 / \partial z^2$ is the Laplace operator.

Since a single source emits in the half-space a flux q , the boundary condition for the Stokes stream function on S_1 , describing a system of one source and two sinks with zero net flux, is $-\frac{\partial \psi}{\partial z} \Big|_{r=0} = \frac{q}{\pi} (\delta(z) - \frac{1}{2} [\delta(z - z_v) + \delta(z + z_v)])$. In order to satisfy $\mathbf{u} \cdot \mathbf{n} = 0$ on S_2 , we take $\psi = \text{constant}$ and $\mathbf{n} \cdot \nabla P = 0$ on S_2 . Without loss of generality, we set $\psi = 0$ on S_2 .

We rewrite (A.3), subject to boundary conditions, in dimensionless form. We choose the following non-dimensional variables: $r = L r'$, $z = L z'$, $\mathbf{u} = U \mathbf{u}'$ and $\psi = q \psi'$, $P = P_{\text{ref}} + P_0 P'$, where $U = q/L^2$ is typical flow velocity scale of maternal blood, $P_0 = \mu q/kL$ is a pressure scale characteristic of the viscous pressure drop across a porous medium, and P_{ref} is a reference pressure intermediate between the arterial and venous pressures (see Table 2). Then the dimensionless problem for blood flow in the hemispherical domain reads:

$$\left. \begin{aligned} \nabla^2 \psi' - \frac{2}{r'} \frac{\partial \psi'}{\partial r'} &= 0, \quad \nabla^2 P' = 0 \quad \text{in } V', \\ -\frac{\partial \psi'}{\partial z'} \Big|_{r'=0} &= \frac{1}{\pi} \left(\delta(z') - \frac{1}{2} [\delta(z' - h) + \delta(z' + h)] \right), \\ -\lim_{r' \rightarrow 0} r' \frac{\partial P'}{\partial r'} &= \frac{1}{\pi} \left(\delta(z') - \frac{1}{2} [\delta(z' - h) + \delta(z' + h)] \right), \end{aligned} \right\} \text{on } S'_1, \quad (\text{A.4})$$

$$\psi' = 0, \quad \frac{\partial P'}{\partial n} = 0 \quad \text{on } S'_2,$$

where $V' = \{|z'| < 1, 0 < r' < 1, 0 < \theta < \pi, r'^2 + z'^2 \leq 1\}$, $S'_1 = \partial V' \cap \{\theta = 0, \theta = \pi\}$, $S'_2 = \partial V' \cap \{r'^2 + z'^2 = 1\}$. The dimensionless source-sink distance is $h = z_v/L$. In the subsequent analysis, the primes over dimensionless variables are dropped.

The fundamental solutions (Green's functions) to the stream function and pressure equations with a singular uniform source at $z = 1$ on the axis of symmetry in an unbounded

domain ($z \in \mathbb{R}$, $r > 0$, $0 \leq \theta < 2\pi$) are as follows [42]:

$$G_\psi = -\frac{1}{4\pi} \frac{z-1}{\sqrt{(z-1)^2 + r^2}}, \quad G_P = \frac{1}{4\pi} \frac{1}{\sqrt{(z-1)^2 + r^2}}. \quad (\text{A.5})$$

The flow and pressure solutions of problem (A.4) in the unbounded half-space $|z| > 0$, $r > 0$, $0 < \theta < \pi$ are given by superposition of the fundamental solutions (A.5) as

$$\begin{aligned} \psi_\infty(r, z) &= -\frac{1}{2\pi} \left(\frac{z}{\sqrt{z^2 + r^2}} - \frac{1}{2} \left[\frac{z-h}{\sqrt{(z-h)^2 + r^2}} + \frac{z+h}{\sqrt{(z+h)^2 + r^2}} \right] \right), \\ P_\infty(r, z) &= \frac{1}{2\pi} \left(\frac{1}{\sqrt{z^2 + r^2}} - \frac{1}{2} \left[\frac{1}{\sqrt{(z-h)^2 + r^2}} + \frac{1}{\sqrt{(z+h)^2 + r^2}} \right] \right). \end{aligned} \quad (\text{A.6})$$

Thus along the z -axis, ψ_∞ takes the values $0, +\frac{1}{2\pi}, -\frac{1}{2\pi}, 0$ as z increases from -1 to $+1$.

The method of images allows us to satisfy the boundary conditions on S_2 by adding a correction to the flow and pressure fields (A.6). In order to do so, we apply Butler's and Weiss's Sphere theorems for axisymmetric fluid motions [42].

Given the unperturbed flow and pressure fields $\psi_\infty(r, z)$, $P_\infty(r, z)$ from (A.6), according to Butler's Sphere theorem [42] the stream function satisfying $\psi = 0$ on S_2 is

$$\psi(r, z) = \psi_\infty(r, z) + \frac{\sqrt{K}}{2\pi} \left(\frac{z}{\sqrt{r^2 + z^2}} - \frac{1}{2} \left[\frac{z-Kh}{\sqrt{r^2 + (z-Kh)^2}} + \frac{z+Kh}{\sqrt{r^2 + (z+Kh)^2}} \right] \right), \quad (\text{A.7})$$

where $K = r^2 + z^2$, $r, z \in V$. The image system consists of two point sinks at inverse points with respect to the sphere ($(r, z) = (0, \pm 1/h)$ for $(0, \pm h)$) and two line sinks, stretched from the inverse points to infinity ($r = 0$, $|z| \geq 1/h$).

By setting $K = 1$ in (A.7) we can readily see that $\psi = 0$ on S_2 as required. One can also check, by direct calculation using (A.7), that the normal component of fluid velocity at the boundary vanishes: $(\mathbf{u} \cdot \mathbf{n}) = \frac{z}{r} \frac{\partial \psi}{\partial r} - \frac{\partial \psi}{\partial z} = 0$ on S_2 .

Application of Weiss's Sphere theorem [42] gives the pressure perturbation in the presence

of a hemisphere:

$$P(r, z) = P_\infty(r, z) + \frac{1}{2\pi} \left(\ln r - \frac{1}{2} \left[\frac{z_v^*}{\sqrt{(z - z_v^*)^2 + r^2}} + \ln \left(\frac{\sqrt{z^2 + r^2} - z}{\sqrt{(z - z_v^*)^2 + r^2} - (z - z_v^*)} \right) + \frac{z_v^*}{\sqrt{(z + z_v^*)^2 + r^2}} + \ln \left(\frac{\sqrt{z^2 + r^2} + z}{\sqrt{(z + z_v^*)^2 + r^2} + (z + z_v^*)} \right) \right] \right), \quad (\text{A.8})$$

where $z_v^* = 1/h$ and $r, z \in V$.

In doing so we obtain exact solutions (A.7), (A.8) to the flow and pressure distributions of boundary-value problem (A.4), as shown in Fig. 3.

We can also find a relation between the (dimensional) source-sink pressure drop $\Delta P = P|_{r=a, z=0} - P|_{r=a, z=z_v}$ (evaluated in the vicinity of the vessel's junctions on the basal plate) and the flow rate q , based on (A.6) for an unbounded domain (in dimensional variables):

$$q = \frac{2\pi k}{\mu} \Delta P \left[\frac{3}{2a} - \frac{2}{\sqrt{a^2 + z_v^2}} + \frac{1}{2\sqrt{a^2 + 4z_v^2}} \right]^{-1} = \frac{4\pi k a}{3\mu} \Delta P \left(1 + O\left(\frac{a}{z_v}\right) \right). \quad (\text{A.9})$$

Here $a \ll z_v$ is the width of a small neighbourhood of a source or sink, of scale comparable with the maternal vessels' radius. We are here exploiting the singular pressure distributions in (A.6) near $z = 0, \pm h$, and are matching the arterial pressure P_a to $P_{\text{ref}} + \mu q / (2\pi k a)$ and venous pressure P_v to $P_{\text{ref}} - \mu q / (4\pi k a)$. Thus we define $P_{\text{ref}} = (P_a + 2P_v) / 3$, with $\Delta P = P_a - P_v$ (e.g. in dimensional variables, for $P_a = 9$ mmHg, $P_v = 3$ mmHg, we have $P_{\text{ref}} = 5$ mmHg and $\Delta P = 6$ mmHg). The relation (A.9) also gives a good approximation in the case of the bounded hemispherical domain: one can show, via expansion in a power series in a , that for $L = 10a$, $z_v = 0.9L$, the relative difference between expression (A.9) and relation based on the precise formula (A.8) is of order 10%. Therefore, the intervillous maternal blood pressure in Fig. 3(c,d) is defined within levels set by the respective radii a of the basal vessels and the fluxes they carry, determining the overall pressure drop ΔP across the placentone.

One can generalise relation (A.9) to the case of the spiral artery (source) and decid-ual veins (sinks) of different radii a_s and a_v respectively, providing that they are sufficiently small and far apart ($a_s, a_v \ll z_v$). The leading order terms in (A.6) give $\Delta P = P|_{r=a_s, z=0} - P|_{r=a_v, z=z_v} \approx \frac{\mu q}{2\pi k} \left(\frac{1}{a_s} + \frac{1}{2a_v} \right)$. Comparing with (A.9), we find the effective ves-

sel's lengthscale a to be a weighted harmonic mean of the source and sinks' lengthscales:

$$a = \frac{3}{2} \left(\frac{1}{a_s} + \frac{1}{2a_v} \right)^{-1}. \quad (\text{A.10})$$

A direct corollary of (A.10) is the dominant influence of the vessels of smaller calibre on the placentone's overall conductance. Indeed, $a \sim 3a_v$ for $a_s \gg a_v$; $a \sim 3a_s/2$ for $a_s \ll a_v$, and $a = a_s$ for $a_s = a_v$.

B. Computation of the solute distribution and net uptake rate

The steady advection-dominated transport of a passive solute in a homogeneous porous medium is described by

$$(\mathbf{u} \cdot \nabla) C = -\alpha C, \quad C|_{r,z=0} = C_0, \quad (\text{B.1})$$

where C is the concentration of a solute (gas or nutrient) in the maternal blood, C_0 is the solute concentration at the source (the spiral artery entering the placentone), α is a solute consumption rate averaged over the pore length scale. According to (B.1), the solute is convected along streamlines (due to relatively large Péclet number, see Table 2).

The concentration distribution of solute $C(r, z)$ in Figs 5 and 6 is computed by numerical integration of the velocity field along streamlines, which are the trajectories of fluid “particles” in the intervillous space. The absolute and relative net uptake rates (shown in Figs S1 and S2) are estimated as a weighted sum of uptakes per unit time over individual streamlines, as explained below.

The steady advective transport of a solute (B.1) is described in dimensionless form (scaling C on C_0 ; primes over dimensionless variables are dropped) by

$$(\mathbf{u} \cdot \nabla) C = -Da C, \quad C|_{r,z=0} = 1, \quad (\text{B.2})$$

where $Da = \alpha L^3/q$ is the Damköhler number.

The concentration distribution of solute is computed by integration of the velocity field along streamlines. We use a Lagrangian formulation to rewrite equation (B.2) as

$$\frac{dC}{dt} = -Da C, \quad C(0) = 1, \quad (\text{B.3})$$

where $C = C(t)$, $\mathbf{x} = (r(t), z(t))$ belongs to a particular streamline, defined as $d\mathbf{x}/dt = \mathbf{u}$, and $t = 0$ at the source ($r = z = 0$). Here t represents time evolution following a material

particle along a streamline. Thus $C(t) = e^{-Dat}$.

The relative net uptake rate of a solute is

$$N_r = 1 - \int_{S_{\text{sink}}} C \mathbf{u} \cdot \mathbf{n} \, dS, \quad (\text{B.4})$$

where S_{sink} is a surface in a small vicinity of the sink and \mathbf{n} is the outward unit normal vector to this surface. The dimensional absolute net uptake rate is $N_a = q C_0 N_r$.

The absolute and relative net uptake rates are estimated using a trapezium quadrature. The time t elapsed since a fluid particle has travelled along a streamline is calculated numerically from $t = \int \frac{ds}{|\mathbf{u}|}$, where s is a distance along the streamline:

$$t = \sum_{i=1}^{n_i} \sqrt{\frac{(\Delta r_i)^2 + (\Delta z_i)^2}{u_r^2(r_i, z_i) + u_z^2(r_i, z_i)}},$$

where $\Delta r_i = r_{i+1} - r_i$, $\Delta z_i = z_{i+1} - z_i$, n_i is the number of points at discretisation of a streamline, velocities u_r and u_z are computed in accord with the definition of the stream function and by use of the exact formula (A.7). The relative computational inaccuracy is of order $1/N$, where N is the number of points of a uniform mesh taken at discretisation in both the z and r directions. Typically 200 streamlines and $N = 800$ uniform grid points are used in the calculations. Linear interpolation between streamlines is used to get a continuous concentration field. Predicted values of N_a and N_r as functions of model parameters are shown in Fig. S1; for discussion see the main text.

An important characteristic of the placentone is the volume fraction of villous tissue ϕ . A qualitative analysis can be performed using the Kozeny–Carman formula for hydraulic conductivity [23]

$$k = \frac{d^2}{180} \frac{(1 - \phi)^3}{\phi^2}, \quad (\text{B.5})$$

where d is an average diameter of villi in the intraplacentone space. Expression (B.5) is most precise for a medium formed by a uniform distribution of solid spheres of constant diameter d .

Using (A.9) and (B.5), we can express the flow rate at the source q in terms of volume fraction, for a constant pressure drop $\Delta P = P|_{r=a, z=0} - P|_{r=a, z=z_v}$ in dimensional variables (evaluated a distance $a = 0.8$ mm from the vessels, where a is comparable to the radius of each vessel; see Table 2), as follows:

$$q(\phi) \simeq \frac{\pi a d^2 \Delta P}{135 \mu} \frac{(1 - \phi)^3}{\phi^2}. \quad (\text{B.6})$$

If we assume that the pressure drop ΔP is constant, and the solute consumption rate per unit volume α is proportional to the surface area of villous tissue, then $q \approx 2q_0(1 - \phi)^3/\phi^2$ and $\alpha \approx 1.6\alpha_0\phi^{2/3}$, where the coefficients of proportionality are chosen in such a way that $\alpha = \alpha_0$, $q = q_0$ at $\phi = 0.5$ (see Table 2). Fig. S2(a) shows the dependence of the absolute net uptake rate N_a (scaled to a reference inlet concentration flux q_0C_0) on ϕ and demonstrates the existence of an optimal volume fraction near $\phi \approx 0.3$.

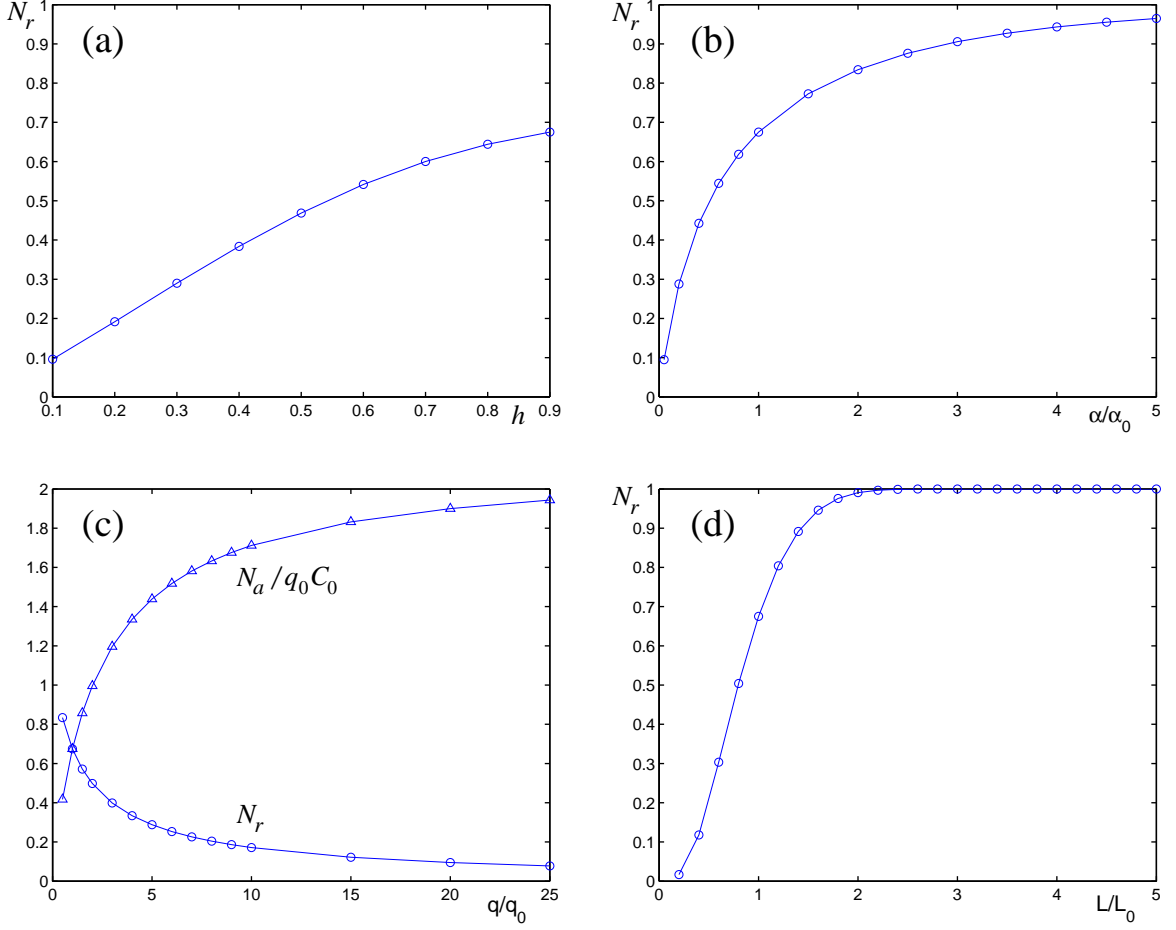


Figure S1. Effect of basal vessels' position and solute consumption rate on a net uptake rate. Dependence of the net uptake rate N_r on: (a) decidual artery-vein distance $h = z_v/L$ ($Da = 1$); (b) solute consumption rate α relative to the reference consumption rate α_0 at fixed inlet flux of maternal blood ($h = 0.9$, $q = q_0$); (c): inlet blood flow rate q relative to the reference flow rate q_0 ($h = 0.9$, $\alpha = \alpha_0$); (d): size of the placentone L relative to the reference placentone radius L_0 ($h = 0.9$, $\alpha = \alpha_0$, $q = q_0$). See Table 2 for parameter values.

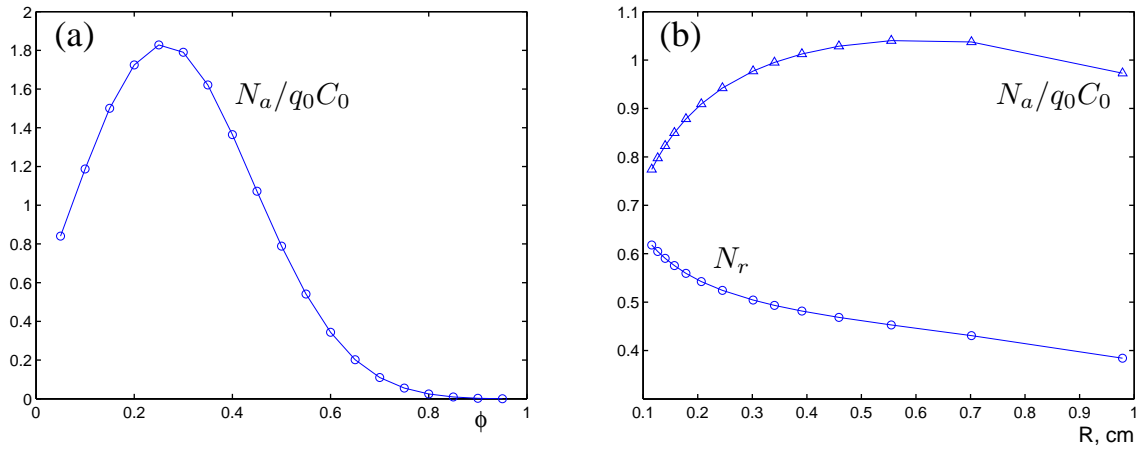


Figure S2. Dependence of absolute net uptake rate N_a on: (a) volume fraction ϕ of homogeneous villous tissue; (b) size of the central cavity R at constant pressure drop ΔP between the basal artery and veins ($h = 0.9$).